

# On Information Plane Analyses of Neural Network Classifiers – A Review

Bernhard C. Geiger

**Abstract**—We review the current literature concerned with information plane analyses of neural network classifiers. While the underlying information bottleneck theory and the claim that information-theoretic compression is causally linked to generalization are plausible, empirical evidence was found to be both supporting and conflicting. We review this evidence together with a detailed analysis how the respective information quantities were estimated. Our analysis suggests that compression visualized in information planes is not information-theoretic, but is rather compatible with geometric compression of the activations.

**Index Terms**—information theory, information bottleneck, information plane analysis, deep learning, deep neural networks

## I. INTRODUCTION AND MOTIVATION

The information bottleneck (IB) theory of deep learning, initially proposed in [1], suggests that a learned latent representation in a neural network (NN) should contain all information from the input required for estimating the target – but not more than this required information. The NN should be *fit* to the target and simultaneously *compress* all irrelevant information to prevent overfitting. If we identify input, target, and latent representations with random variables (RVs)  $X$ ,  $Y$ , and  $L$  respectively, then  $L$  should be a *minimal sufficient statistic* for  $Y$  obtained from  $X$ . In information-theoretic terms, this is equivalent to finding a latent representation  $L$  that minimizes the mutual information  $I(X; L)$  with the input  $X$  while satisfying  $I(L; Y) = I(X; Y)$ . Since the minimizing  $L$  may not be obtainable with a NN of a given architecture, one can relax the problem to the IB problem:

$$\min_{P_{L|X}} I(X; L) - \beta I(Y; L) \quad (1)$$

where  $\beta$  trades between preserving target-relevant information and compressing target-irrelevant information. Indeed, for the case of an input  $X$  with finite alphabet, the authors of [2] have shown that an estimate of  $I(X; L)$  from the dataset appears in a bound on the generalization error.

The work of Bernhard C. Geiger was supported by the iDev40 project. The iDev40 project has received funding from the ECSEL Joint Undertaking (JU) under grant agreement No 783163. The JU receives support from the European Unions Horizon 2020 research and innovation programme. It is co-funded by the consortium members, grants from Austria, Germany, Belgium, Italy, Spain and Romania. The Know-Center is funded within the Austrian COMET Program - Competence Centers for Excellent Technologies - under the auspices of the Austrian Federal Ministry of Transport, Innovation and Technology, the Austrian Federal Ministry of Digital and Economic Affairs, and by the State of Styria. COMET is managed by the Austrian Research Promotion Agency FFG.

Bernhard C. Geiger is with Know-Center GmbH, 8010, Graz, Austria (e-mail: geiger@ieee.org).

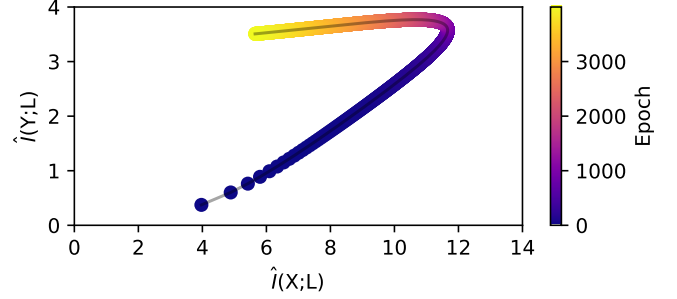


Fig. 1. Faux information plane for one NN layer. Three consecutive phases are visible: fitting (increase of  $\hat{I}(Y; L)$ ), compression (decrease of  $\hat{I}(X; L)$ ), and overfitting (small decrease of  $\hat{I}(Y; L)$ ).

Based on the IB theory, the authors of [3] popularized the analysis of the *information plane* (IP), in which estimates of the two quantities  $I(X; L)$  and  $I(Y; L)$  are the coordinate axes (see Fig. 1). The IP is used to visualize how the estimates of  $I(X; L_t)$  and  $I(Y; L_t)$  change with the training epoch  $t$ ; e.g., *fitting* to the target is indicated by an increase of the estimate of  $I(Y; L_t)$  as  $t$  increases, and *compression* is characterized by a decrease of the estimate of  $I(X; L_t)$ . For example, the authors of [3] observed that training a NN with SGD is characterized by a short fitting phase followed by a long compression phase, which the authors claimed to be connected to generalization. This enticing idea, that the reason behind good generalization performance can simply be read off a chart, led to the belief that IP analyses could reveal more about the inner workings of NNs – that they may “open the black box of deep learning”.

Several authors have subsequently performed IP analyses, applying different estimation mechanisms to different NN architectures. The evidence they obtained was conflicting: For example, the authors of [4] did not observe compression at all for NNs with ReLU activation functions, and the authors of [5] observed compression sometimes at an earlier phase, sometimes at a later phase of training, depending on the initialization of the NN parameters. Also, the link between compression and generalization has been questioned, cf. [4].

It is the goal of this paper to summarize and consolidate these partly conflicting observations. We start by discussing the complications of estimating mutual information in deterministic NNs in Section II and argue that IP analyses obtained with different estimators are not directly comparable. Building upon this insight, we survey IP analyses of NNs in Section III. Throughout this section, we observe that geometric compression, i.e., that  $L$  is “small” or densely clustered in latent space, is a plausible explanation for compression in the IP; this is in line with previous work [6], [7]. Further,

we conclude in Section IV that the evidence presented for the *presence* of a causal link between compression in the IP and good generalization performance is less convincing than the evidence presented for its *absence*. Based on these conclusions, we discuss the validity and value of IP analyses, indicating that they can nevertheless shed significant light on the training process of a NN, given that the specifics of mutual information estimation are properly taken into account.

**Considered Literature and Scope:** We exclusively consider work investigating the behavior of (estimates of)  $I(X; L_t)$  and  $I(Y; L_t)$  during training of NN classifiers; see Table I for an overview. We do not consider information-theoretic analyses of trained NNs, such as [20], [21]; works concerned with the mutual information between the network input (data)  $X$  ( $\mathcal{D}$ ) and the network weights, such as [22]; IP analyses of neural auto-encoders or NNs trained for regression; and the interesting body of literature concerned with information-theoretic objectives for NN training, such as [23]–[25]. However, the fast pace at which this scientific field progresses requires us to consider (currently still) unpublished work in addition to work that has passed peer-review. That such an approach is accepted by the scientific community sees evidence in the fact that [3] has accumulated more than 400 citations, but has not yet passed peer-review.

**Notation:** We let  $X$  and  $Y$  denote RVs representing the features and target of a classification problem. Typically,  $X$  has a continuous distribution on a high-dimensional space, while  $Y$  has a discrete distribution on a finite set of classes. The dataset  $\mathcal{D} = \{(x_1, y_1), \dots, (x_N, y_N)\}$  is assumed to contain independent realizations of the joint distribution of  $X$  and  $Y$ . The features  $X$  are the input to a NN. We describe each NN by the widths of the hidden layers and let the input and output dimensions be defined from the context. For example, 1024 – 512 – 256 is a multilayer perceptron (MLP) with three hidden layers of widths 1024, 512, and 256, respectively. The output of a layer or filter inside the NN at epoch  $t$  defines the latent representation  $L_t$ ; we suppress the epoch index  $t$  for the sake of readability. We use indices, e.g.,  $L_i, L_j, \dots$ , to refer to latent representations of different layers. We call a NN *deterministic* if it implements a function  $f$  from the input  $X$  to the latent representation  $L$ , i.e., if  $L = f(X)$ . We call a NN *stochastic* if it implements a conditional distribution. We let  $I(\cdot; \cdot)$ ,  $H(\cdot)$ ,  $\hat{I}(\cdot; \cdot)$ , and  $\hat{H}(\cdot)$  denote mutual information, entropy, and their estimates, respectively.

## II. MUTUAL INFORMATION IN NEURAL NETWORKS

Since the IP displays how  $I(X; L)$  and  $I(Y; L)$  change during training, these quantities need to be estimated from the dataset  $\mathcal{D}$ . This is at least theoretically possible if the quantities  $I(X; L)$  and  $I(Y; L)$  are finite. For example,  $I(Y; L)$  is finite for classification tasks in which  $Y$  is a RV on a finite set  $\mathcal{Y}$  of classes. Thus, one can reasonably assume that  $\hat{I}(Y; L) \approx I(Y; L)$  if the estimator is adequately parameterized. For example, if  $Q(\cdot)$  is a quantizer, then the plug-in estimate for

$I(Y; L)$  obtained from dataset  $\mathcal{D}$  yields

$$\begin{aligned} \hat{I}(Y; L) &= I(Y; Q(L)) \\ &= \sum_{q \in \text{range}(Q)} \sum_{y \in \mathcal{Y}} \hat{p}_{Y, Q(L)}(y, q) \log \frac{\hat{p}_{Y, Q(L)}(y, q)}{\hat{p}_{Q(L)}(q) \hat{p}_Y(y)} \end{aligned} \quad (2a)$$

where  $\hat{p}_{Y, Q(L)}(y, q) = |\{i: f(x_i) = q, y_i = y\}|/|\mathcal{D}|$ , and where  $\hat{p}_{Q(L)}$  and  $\hat{p}_Y$  are obtained by marginalizing  $\hat{p}_{Y, Q(L)}$ . Then,  $\hat{I}(Y; L) \approx I(Y; L)$  if  $Q$  has appropriate bin size and if  $\mathcal{D}$  is sufficiently large.

There are settings in which also  $I(X; L)$  is finite, cf. Section 5 in [26]. For example,  $I(X; L)$  is finite if the latent representation  $L = \hat{Y}$  is the (finite-alphabet) class-estimate of the NN. Also, if the NN is stochastic, as in scenarios where  $f$  is a probability distribution parameterized by a NN,  $I(X; L)$  is finite. In these cases, an IP analysis is uncontroversial, given that the estimators can be parameterized such that their estimates are close to the true (finite) quantities.

However, if the NN is deterministic, estimating the mutual information  $I(X; L)$  (which coincides with the entropy  $H(L)$  in this case) is problematic, if not futile. To make this clear, we discuss two common assumptions regarding the distribution  $P_X$  of the features  $X$ .

In the first case, we assume that the distribution  $P_X$  is continuous.<sup>1</sup> If the NN is such that also  $L$  has a continuous distribution, then one can easily show that  $I(X; L) = \infty$  [4], [6]. More rigorously, Th. 1 in [26] shows that  $I(X; L) = \infty$  for continuous  $X$  and many common activations functions (incl. tanh, sigmoid, or leaky ReLU), even if  $L$  is not continuous.

In the second case, we assume that the features follow the empirical distribution of the dataset  $\mathcal{D}$ , i.e., the distribution  $P_X$  has a point mass at the position of every sample from the dataset  $\mathcal{D}$ . In this case, most NNs will map the dataset bijectively, i.e., if the features of two samples in the dataset are distinct, then with high probability so will be all their latent representations – this is a simple consequence of the fact that  $|\mathcal{D}|$  is usually much smaller than the cardinality of the feature space and the fact that most activation functions have a strictly monotonous part. Under this assumption on  $P_X$ , one has  $I(X; L) = \log |\mathcal{D}|$  and  $I(Y; L) = I(Y; X)$ .

In contrast, the *estimator* of mutual information typically yields different results: For example, if  $Q(\cdot)$  is a quantizer with large bin size and if  $L$  is low-dimensional, the plug-in estimate for  $I(X; L)$  obtained from dataset  $\mathcal{D}$  yields

$$\begin{aligned} \hat{I}(X; L) &= I(X; Q(L)) = H(Q(L)) \\ &= - \sum_{q \in \text{range}(Q)} \hat{p}_{Q(L)}(q) \log \hat{p}_{Q(L)}(q) \ll \log |\mathcal{D}| \end{aligned} \quad (2b)$$

where  $\hat{p}_{Q(L)}(q) = |\{i: f(x_i) = q\}|/|\mathcal{D}|$ . If the bin size is small or if  $L$  is high-dimensional, as in a convolutional NN (CNN), then one may observe  $\hat{I}(X; L) \approx \log |\mathcal{D}|$  and  $\hat{I}(Y; L) \approx \hat{H}(Y)$  because almost all data points fall into different bins; cf. Fig. 15 in [4] and Fig. 1 in [6]. From this

<sup>1</sup>A discrete distribution on a high-dimensional finite space is appropriately modeled as being continuous. E.g., for image classification, the pixel  $X_i$  has a discrete distribution on  $\{0, \dots, 255\}$ <sup>3</sup> that is modeled as a continuous distribution on  $[0, 1]$ <sup>3</sup>.

TABLE I

OVERVIEW OF THE SURVEYED LITERATURE. THE LAST TWO COLUMNS INDICATE WHETHER COMPRESSION (COMP) WAS OBSERVED ( $\checkmark$ ), WAS NOT OBSERVED ( $\times$ ), OR WHETHER THE PICTURE WAS INCONSISTENT ( $\sim$ ); AND WHETHER THE AUTHORS MADE SUPPORTING ( $\checkmark$ ), NEGATING ( $\times$ ), OR BOTH TYPES ( $\sim$ ) OF CLAIMS FOR A CAUSAL LINK BETWEEN COMPRESSION AND GENERALIZATION (GEN). IT CAN BE SEEN THAT COMPRESSION IS LESS COMMON THAN EXPECTED, AND THAT ITS CONNECTION WITH GENERALIZATION HAS BEEN QUESTIONED. WE USED THE FOLLOWING ABBREVIATIONS: BATCH GRADIENT DESCENT (BGD), BINNING (BIN), DENSENET (DN), FASHIONMNIST (F-MNIST), LeNet (LN), SIGMOID (SIG.), STOCHASTIC GRADIENT DESCENT (SGD), SYNTHETIC DATASET (SYN.), TRAINING METHOD (TRAIN.), VARIATIONAL (VAR.). THE TERM ‘‘ALL’’ IN THE COLUMN FOR THE TRAINING METHOD INDICATES THAT SGD, BGD, AND ADAM WERE USED FOR TRAINING IN DIFFERENT EXPERIMENTS.

REFERENCE	ARCHITECTURE	ACTIVATION	TRAIN.	DATASET	ESTIMATOR	COMP	GEN
[8], [9]	MLP, LN, DN	tanh, sig., ReLU	SGD	MNIST, CIFAR, SYN.	DECISION RULE	$\times$	
[5]	MLP	tanh, ReLU	ADAM	SZT	BIN, KDE	$\sim$	$\sim$
[10]	MLP, CNN	SOFTMAX	ALL	MNIST, CIFAR-10	BIN	$\sim$	$\checkmark$
[11]	RESNET	LEAKY ReLU	SGD	CINIC-10	VAR.	$\checkmark$	
[12]	MLP	tanh, ReLU	ADAM	MNIST	MINE	$\sim$	
[13]	MLP, LN, DN	ReLU	ADAM	MNIST	KDE	$\sim$	
[14]	MLP	HARDTAN, ReLU	SGD	SYN.	REPLICA	$\sim$	$\times$
[6]	MLP, CNN	tanh, ReLU	SGD	SZT, MNIST, SYN.	BIN, OWN	$\sim$	$\times$
[15]	VGG16	ReLU	?	CIFAR-10	MINE	$\checkmark$	
[16]	MLP, CNN	tanh, ReLU	ADAM	MNIST	BIN + HASH	$\checkmark$	
[3]	MLP	tanh	SGD	SZT	BIN	$\checkmark$	$\checkmark$
[4]	MLP	tanh, ReLU, LIN.	SGD, BGD	SZT, MNIST, SYN.	BIN, KDE	$\sim$	$\times$
[7]	MLP	tanh, ReLU	SGD	SZT, MNIST	BIN	$\sim$	$\times$
[17]	MLP, CNN	ERF, ReLU	?	MNIST, SYN.	VAR., SAMPLE	$\times$	$\times$
[18]	MLP, CNN, VGG16	tanh, ReLU	SGD	MNIST, CIFAR-10	KERNEL	$\sim$	$\times$
[19]	LN	SIG.	SGD	MNIST, F-MNIST	KERNEL	$\times$	

becomes apparent that the definition of the quantizer  $Q$  has profound effect on the results obtained by such information-theoretic analyses; similar considerations hold if  $\hat{I}(X; L)$  is not computed using binning, but, e.g., using kernel-density estimators (KDE). This has an immediate consequence for IP analyses: First,  $\hat{I}(X; L)$  and  $\hat{I}(Y; L)$  depend on the choice of the estimator, IPs can only be interpreted with the details of estimation in mind. Second, and more importantly, IPs obtained by different estimators are not directly comparable. Conflicting claims made on the basis of IP analyses can only be conflicting if the same estimators are used; if different estimators are used, conflict or agreement is only superficial, since the IPs show different things despite identical axis labelling.

### III. INFORMATION PLANE ANALYSES OF NEURAL NETWORKS

In the following subsections, we critically survey the current literature on IP analyses, categorized according to the type of mutual information estimation. For the sake of readability, we use  $\hat{I}(\cdot; \cdot)$  for every estimator; critical statements regarding estimation are therefore only valid within the same context (e.g., paragraph, subsection,...). Furthermore, we implicitly assume that a NN is deterministic. If it is not, then we explicitly declare it as stochastic.

#### A. Binning Estimators

Binning estimators first apply a quantizer  $Q$  to the latent representation  $L$  and/or the input  $X$  and then compute  $\hat{I}(X; L)$  and  $\hat{I}(Y; L)$  for the binned RVs using the plug-in estimator in (2).

The most prominent work in this category is [3], in which the authors ran experiments with a 10–7–5–4–3 MLP with tanh activation functions. During training, they used SGD to minimize the cross-entropy loss in a binary classification task on a synthetic dataset of dimensionality 4096; we henceforth

refer to this dataset as SZT. The quantizer  $Q$  was chosen such that it uniformly quantizes the range of each neuron output into 30 bins. The authors observed that, during training,  $\hat{I}(Y; L)$  initially increases fast (fitting phase), while later  $\hat{I}(X; L)$  decreases slowly – SGD *compressed* information about the features  $X$ . This led to the claim that SGD runs in two phases, a drift and a diffusion phase, that are purportedly connected with fitting and generalization, respectively. Also, when training with little training data, the network appears to overfit, which is visible in the IP as a late decrease of  $\hat{I}(Y; L)$ . cf. Fig. 1.

Subsequently, most claims in [3] have been challenged. For example, it was shown that compression also happens when training with Adam, cf. [5] and full-batch gradient descent, cf. [4]. Thus, SGD is not the (only) reason behind compression in the IP, although it was observed to cause stronger compression than Adam in the softmax layer, cf. Fig. 12 in [10]. Similarly, the two-phase nature of NN training has been questioned, as the authors of [5] have observed that, depending on the random initialization of the NN,  $\hat{I}(X; L)$  may first decrease before increasing, first increase before decreasing, only increase, or not change at all. Also the authors of [6] observed that  $\hat{I}(X; L)$  may increase and decrease again multiple times throughout training a stochastic 10–7–5–4–3 MLP. The authors of [10] showed that the softmax layer of various NN architectures exhibits a compression phase when the NNs are trained on MNIST, but that the CIFAR-10 dataset is too complex to allow compression in shallow NNs (such as a three-layer MLP and two- or four-layer CNNs).

The interplay between bin size and NN architecture has a great effect on the qualitative picture delivered by the IP, cf. discussion after (2b). For example, the authors of [7] observe that for small bin sizes, many deep layers remain at the point  $(\log |\mathcal{D}|, I(X; Y))$  in the IP throughout training, indicating that every sample of  $\mathcal{D}$  falls into a different bin. Indeed, for a 1024 – 20 – 20 – 20 MLP with ReLU activation functions

trained on MNIST, uniform binning with a bin size of 0.5 yielded that  $\hat{I}(X; L)$  converges to  $\log |\mathcal{D}|$  for every layer, cf. Fig. 10 in [4]. Similarly, for a CNN (two convolutional layers and two fully connected layers with widths 1583–128) with tanh activation functions trained on MNIST using noise regularization, the authors of [6] showed that for all layers  $\hat{I}(X; L) = H(Q(L)) \approx \log |\mathcal{D}|$  with only binary quantization. Larger bin sizes, on the other hand, lead to more samples falling into the same bins, especially for narrow layers. This explains why  $\hat{I}(X; L)$  decreases with the layer index in the 10–7–5–4–3 MLP, cf. [3], [7]. In contrast to common belief, this decrease is not a consequence of the data processing inequality. While  $X - L_1 - L_2 - \dots - L_m$  is a Markov tuple, the same does not hold for the binned RVs  $Q(L_i)$ . Hence,  $\hat{I}(X; L_1) \geq \hat{I}(X; L_2) \geq \dots \geq \hat{I}(X; L_m)$  need not hold for binning estimators. Indeed, for a 12–3–2–12–2–2 MLP the authors of [7] showed that  $\hat{I}(X; L_3) < \hat{I}(X; L_4)$  throughout entire training, which is caused by the fact that the third hidden layer has less dimensions than the fourth, thus also less options to map data points to different bins.

Also the fact whether compression occurs at all has been questioned by several authors. The authors of [4], [7] argue that compression is a consequence of combining the binning estimator with doubly saturating nonlinearities (see, e.g., Fig. 2 in [4]). For tanh activation functions, during training less and less bins are used, i.e., the tanh activation values saturate; this claim is backed by histograms over activation values in [4], [7]. In contrast, the ReLU activation values start at small values initially because of random weight initialization, but then increase to larger values, i.e., the total range of activation values increases, cf. Fig. 5 in [7]. This leads to a noticeable increase of  $\hat{I}(X; L)$  when  $Q$  is a quantizer with a fixed bin size. Consequently, the authors of [4], [6], [7] observe compression in MLPs with tanh activation functions trained on SZT and MNIST, but not if ReLU activation functions were used. The authors of [5] observed compression for *some* randomly initialized NNs with ReLU activation functions, but not *on average*. NNs with ReLU activation functions display compression in the IP if weight decay is used for regularization [5], indicating that weight decay has the potential to “saturate” the ReLU activation function in the sense of making many neurons inactive. In contrast, regularization encouraging orthonormal weight matrices prevents compression in stochastic NNs with tanh activation functions [6].

Finally, there has also been evidence that compression may not be linked to generalization: In [4], two deep linear teacher-student networks, one generalizing well and one suffering from overfitting, did not exhibit compression, while compression occurred in a strongly overfitted NN with tanh activation functions. The authors of [7] claim that there may be a connection between early stopping and the start of the compression phase, but not between generalization and compression. Also the authors of [5] and the authors of [6] do not observe any connection between compression of a hidden layer and generalization. Indeed, especially for wide hidden layers or convolutional layers it was often observed that  $\hat{I}(X; L) \approx \log |\mathcal{D}|$  [4], [6], [27]. In other words, these NNs are almost invertible on the test dataset. Since they are still capable

of achieving state-of-the-art results, compression in the IP cannot be necessary for good generalization performance. This is in line with recent results on NNs that are invertible by design [28], [29].

In contrast to this, the authors of [5] observe that generalization seems to be correlated with compression in the final softmax layer. The authors of [10], [30] arrived at the same conclusion by investigating pairs of points in the IP of a VGG-16 trained on CIFAR-10: If  $\hat{I}(Y; L)$  is the same for both points but one point has higher accuracy, then this point is often characterized by a lower value of  $\hat{I}(X; L)$ ; i.e., compression, measured by uniformly binning the softmax layer into ten bins, is correlated with improved generalization performance. This is plausible, as the softmax layer represents the confidence that a sample from  $\mathcal{D}$  belongs to a certain class. As the NN gains confidence, fewer and fewer quantization patterns become possible, thus reducing  $\hat{I}(X; L)$ .

The results of this section are difficult to compare with each other: In [3], [6], [7], the quantizer  $Q$  is fixed; for some results in [4] it is adapted to the training run; and in [5] it is adapted to every layer and every epoch: In their binning scheme, bin boundaries are placed at the percentiles of the empirical activation value distribution for each epoch and each layer. In other words,  $Q$  is the maximum output entropy quantizer [31]. This quantizer is not uniform, as the bins are more narrow in regions where data points accumulate. This makes the results in [5] particularly difficult to interpret. In any case, a reduction of  $\hat{I}(X; L) = H(Q(L))$  is only possible if multiple data points are mapped to the same bin by the NN function  $f$ . If  $Q$  is fixed, one possible cause for many data points being mapped to the same bin is the image of  $\mathcal{D}$  under  $f$  having a small diameter. Another cause is that  $f$  maps  $\mathcal{D}$  to few dense clusters. Both types of geometric compression – clustering or shrinking – are thus possible explanations for compression observed in the IP. Simultaneously, clustering is an explanation for fitting, i.e., for an increase of  $\hat{I}(Y; L)$ : If  $f$  maps samples from each class in  $\mathcal{D}$  to a different cluster and if  $Q$  is such that no two clusters are mapped to the same bin, then  $\hat{I}(Y; L) = H(Y)$ , which is the maximum achievable value. Thus, geometric clustering according to class membership can explain both fitting and compression phases observed in the IP. Figs. 5a and 8 in [6] provide evidence for this explanation by showing that the latent representation  $L$  is geometrically clustered in epochs with small  $\hat{I}(X; L)$  and that during training the distances between samples within the same class become significantly smaller than the distances between samples of different classes.

## B. Kernel Density Estimation (KDE)

The authors of [4] also used KDE to estimate mutual information; specifically, they relied on the KDE proposed in [32], which assumes the addition of Gaussian noise  $\varepsilon$  of variance  $\sigma^2$  and provides the following upper and lower

bounds:

$$\begin{aligned}
& -\frac{1}{|\mathcal{D}|} \sum_i \log \frac{1}{|\mathcal{D}|} \sum_j \exp \left( -\frac{1}{2} \frac{\|f(x_i) - f(x_j)\|_2^2}{4\sigma^2} \right) \\
& \leq \hat{I}(X; L) = I(X; L + \varepsilon) \\
& \leq -\frac{1}{|\mathcal{D}|} \sum_i \log \frac{1}{|\mathcal{D}|} \sum_j \exp \left( -\frac{1}{2} \frac{\|f(x_i) - f(x_j)\|_2^2}{\sigma^2} \right) \quad (3)
\end{aligned}$$

They admit that “the addition of noise [in KDE] means that different architectures may no longer be compared in a common currency of mutual information”. And indeed, their results indicate that their upper bound on  $\hat{I}(X; L)$  often lies *below* the value  $\hat{I}(X; L)$  obtained via binning, which is known to be a lower bound on the true mutual information; see Figs. 9 & 10 in [4].

Paralleling our discussion on the effect of the bin size in Section III-A, we observe that the setting of the variance  $\sigma^2$  strongly influences the qualitative picture conveyed by the IP. For example, with  $\sigma^2 = 0.1$ , the authors of [4] showed that compression occurs in a 10 – 7 – 5 – 4 – 3 MLP trained on SZT and a 1024 – 20 – 20 – 20 MLP trained on MNIST only if tanh activation functions are used. No compression was observed for NNs with ReLU activation functions; for the MNIST setting,  $\hat{I}(X; L)$  eventually converged to  $\log |\mathcal{D}|$  for all layers. In contrast, the authors of [5] observed compression in a later phase of training a 10 – 7 – 5 – 4 – 3 MLP with ReLU activation functions on SZT; they adapted, for each epoch,  $\sigma^2$  to the maximum activation of the layer. Finally, the authors of [13] used the KDE to estimate the IP for a 1024 – 256 – 128 MLP with ReLU activation functions, a LeNet-5, and a DenseNet, each trained on the MNIST dataset. Their results are inconclusive regarding compression, but all indicate that  $\hat{I}(Y; L)$  increases throughout training, albeit not necessarily monotonically, cf. Fig. 4 in [13]. Interestingly, the authors claim that all three networks achieve test set accuracies exceeding 95%, indicating  $I(Y; L) \approx \log 10$ , yet even after 50000 epochs the NNs final layers saturate at around  $\hat{I}(Y; L) = 1, 2, \text{ or } 3$  bit, respectively. These facts can only be consolidated by noting that the KDE is a poor estimator of  $I(Y; L)$  in this case, e.g., because the variance  $\sigma^2$  of the Gaussian noise  $\varepsilon$  was chosen too large.

Looking at the definition of the KDE in (3), one observes that geometry plays a fundamental role in estimating mutual information: The estimate relies on the pairwise distances between images of data points under the NN function  $f$ . And indeed, as the authors of [32] show, the upper and lower bounds in (3) are tight if the data points are perfectly clustered, i.e., if mapped data points are either very close to each other (within the same cluster) or very far apart (in different clusters). Furthermore, using a fixed variance  $\sigma^2$  in (3) applies a fixed measurement scale, and changing the absolute scale of the activation values  $L$  relative to this variance leads to compression in the IP; see, e.g., Fig. 1A in [32]. At the same time, clustering  $\mathcal{D}$  according to class membership and moving these clusters far apart is a plausible explanation for an increase of  $\hat{I}(Y; L)$ . Since in [5] the variance  $\sigma^2$  is adapted to the activation values, a decrease of  $\hat{I}(X; L)$  can be explained

by clustering, but not by scaling. Thus, clustering appears to be a valid explanation for compression observed in IP analyses based on KDE.

### C. Variational and Neural Network-Based Estimators

Variational estimators of mutual information are obtained by optimizing a parameterized bound on mutual information over a restricted feasible set. For example, a variational lower bound on mutual information is obtained via eq. (2) in [33]

$$I(Y; L) = \mathbb{E} \left[ \frac{p_{Y|L}(Y|L)}{p_Y(Y)} \right] \geq \mathbb{E} \left[ \frac{q_{Y|L}(Y|L)}{p_Y(Y)} \right] \quad (4)$$

where the expectation is over the joint distribution of  $Y$  and  $L$  and where  $q_{Y|L}$  is parameterized by, e.g., a NN that is optimized to maximize this lower bound. For example,  $q_{Y|L}$  could be the distribution determined by a NN classifier with input  $L$ , while  $q_{X|L}$  could be a generative model [11]. Another type of variational lower bound can be obtained from the Donsker-Varadhan representation of mutual information, which is the principle underlying MINE [34].

MINE was used to estimate the IPs in [12] and [15] for a 784 – 512 – 512 – 10 MLP with ReLU or tanh activation functions trained on MNIST and a VGG-16 CNN trained on CIFAR-10, respectively. Reference [11] used a NN classifier and a generative PixelCNN++ [35] as variational distributions for analysing the IP of a ResNet trained on CINIC-10. While the authors of [12] added Gaussian noise  $\varepsilon$  with variance  $\sigma^2 = 2$  for the purpose of estimation, the other authors appear not to have added noise. The qualitative pictures are entirely different: The authors of [15] observe compression from the first epoch; the authors of [11] observe compression (which is stronger for early layers) at the end of training; [12] do not observe compression at all, unless weight decay is used for regularization, cf. Fig. 2 in the supplementary material of [12]. All authors observe a fitting phase in the sense that  $\hat{I}(Y; L)$  increases. However, while Fig. 1a in [15] shows that  $\hat{I}(Y; L)$  increases to  $\log 10$  from a comparably large starting value, in [12]  $\hat{I}(Y; L)$  appears to reach a much smaller value of only 2.2 bit at the end of training.

These variational estimates are hard to interpret. The images generated using PixelCNN++ from deeper latent representations  $L$  are more diverse within the same class than those generated from earlier layers, cf. Figs. 4, 5, and 7 in [11]; similarly, class-irrelevant features seem to be discarded throughout training. Although the images generated using PixelCNN++ are in good agreement with the IP, it is questionable in how far this admits conclusions regarding the latent representations  $L$ . Indeed, the authors admit that their estimate  $\hat{I}(X; L)$  is restricted to the “level of usable information, in as much as it can recover the images”. At least, there is no reason to believe that a reduction of  $\hat{I}(X; L)$  estimated using a generative model can plausibly be explained by geometric compression. Similar considerations hold for the IP in [15] which violates the data processing inequality:  $\hat{I}(X; L) < \hat{I}(Y; L)$  for layer 16 at the end of training, cf. Fig. 1 in [15]. Only the authors of [12] acknowledge that  $I(X; L) = \infty$ , in which case MINE is known to yield a poor estimate (Fig. 1, right in [34] or

Fig. 1 in [12]). The authors thus adapt MINE and estimate  $I(X; L + \varepsilon)$  which, with a constant noise variance, is a measure for geometric compression. And indeed, since small (initial) weights reduce the range of the layer output  $L$ , this geometric compression explains why  $\hat{I}(X; L) \approx 0$  at the beginning of training and why weight decay leads to compression in the IP.

#### D. Kernel-Based Estimators

Reference [19] uses a matrix-based analog of entropy

$$\hat{H}_\alpha(X) = S_\alpha(A) = \frac{1}{1-\alpha} \log \text{tr}(A^\alpha). \quad (5a)$$

where matrix  $A$  is such that  $A_{i,j} = \frac{1}{|\mathcal{D}|} \frac{G_{i,j}}{\sqrt{G_{i,i}G_{j,j}}}$  and where  $G$  is the Gramian is obtained by evaluating a Gaussian kernel for all pairs of points in  $\mathcal{D}$ . Shannon entropy is obtained by letting  $\alpha \rightarrow 1$ ; the authors have chosen  $\alpha = 1.01$ . Mutual information, e.g., between the input  $X$  and a convolutional layer  $L = (L_1, \dots, L_c)$  with  $c$  filters, is computed by setting

$$\hat{I}(X; L) = S_{1.01}(A) + S_{1.01} \left( \frac{A_1 \circ \dots \circ A_c}{\text{tr}(A_1 \circ \dots \circ A_c)} \right) - S_{1.01} \left( \frac{A \circ A_1 \circ \dots \circ A_c}{\text{tr}(A \circ A_1 \circ \dots \circ A_c)} \right) \quad (5b)$$

where  $A_i$  is obtained from the Gramian of  $L_i$  and where  $\circ$  denotes the Hadamard product. These Hadamard products become numerically problematic for CNNs with many filters, which is why the authors of [18] have proposed the use of tensor kernels in the computation of  $A$  instead.

The authors of [19] performed experiments with a LeNet-5 trained on MNIST and FashionMNIST using SGD. Despite using doubly saturating sigmoid activation functions, the authors did not observe any compression phase in the IP. Rather, both  $\hat{I}(X; L)$  and  $\hat{I}(Y; L)$  increase rapidly. Similarly, the authors of [18] observe compression only in the softmax layer of a CNN with three convolutional layers and two fully connected layers with widths 400 – 256 trained on MNIST, while for the preceding layers  $\hat{I}(X; L)$  and  $\hat{I}(Y; L)$  stay at high values throughout entire training. In contrast, the authors of [18] observe fitting and subsequent compression in a 1000 – 20 – 20 – 20 MLP trained on MNIST regardless whether ReLU or tanh activation functions are used<sup>2</sup> and in deeper layers of a VGG-16 trained on CIFAR-10. Further, the authors of [18] show that at the end of training all layers of the MLP and the CNN have  $\hat{I}(Y; L) \approx \log(10)$ , indicating that the NNs have learned successfully. For the VGG-16, however,  $\hat{I}(Y; L)$  is lower when evaluated on the test set than on the training set, which is explained by slight overfitting.

Indeed, also the compression observed in [18] can be explained by geometric clustering: If  $x_i \approx x_j$  for two data points in the same class, but if  $x_i$  and  $x_j$  are sufficiently far apart if the class labels are different, then the matrix  $A$  is approximately block-diagonal with a rank well approximated by the number of classes (cf. discussion leading to eq. (10) in [18]). Therefore, a decrease in  $\hat{I}(X; L)$  can be explained by

<sup>2</sup>The violation of the data processing inequality in Figs. 2 & 3 in [18], in the sense that  $\hat{I}(X; L) < \hat{I}(Y; L)$  for the softmax layer at the end of training, can be explained by different kernel widths chosen for either estimator.

data points from the same class moving closer together, and data points from different classes moving further apart.

#### E. Other Estimators

Aside from binning, KDE, and NN-based estimation, several other estimation schemes have been proposed and applied to IP analyses of NNs. For example, [14] uses the replica method from statistical physics to estimate the differential entropy (and mutual information) in NNs with wide layers and random, independent and orthogonally-invariant weight matrices. To make the estimate (which is exact in the linear case) finite, they assume that Gaussian noise  $\varepsilon$  with variance  $\sigma^2 = 10^{-5}$  was added to  $L$ , i.e., they estimate  $\hat{I}(X; L) = I(X; L + \varepsilon)$ ; the NN is otherwise deterministic. They perform experiments with a 1000 – 500 – 250 – 100 MLP designed to satisfy the orthogonal invariance of the weight matrices. For NNs with mixed activation functions (linear and ReLU or linear and hardtanh) trained on a synthetic dataset, the authors observe that  $\hat{I}(X; L)$  is always decreasing, potentially after an short initial increase. For NNs with only hardtanh activation functions, the behavior is less consistent and depends on the variance of the initial weights. The source of this compression is hard to determine; since  $\hat{I}(X; L)$  is an estimate of  $I(X; L + \varepsilon)$ , a certain geometric influence cannot be ruled out. In any case, since an eventual compression is not synchronized with generalization, Gabri e et al. conclude that compression and generalization may not be linked and that within their examined setting “a simple information theory of deep learning [may remain] out-of-reach”.

In [17], the authors consider infinite ensembles of infinitely wide deterministic NNs initialized with Gaussian weights, for which it is shown that minimizing the square loss makes the distribution  $P_{L|X}$  Gaussian for every epoch. Thus, the ensemble is stochastic with finite mutual information values and they estimate  $I(X; L)$  and  $I(Y; L)$  via multi-sample and variational bounds. Their experiments with an ensemble of 1000 – 1000 – 1000 MLPs trained on a Gaussian regression dataset do not show compression in the IP, but indicate that overfitting is represented by decrease of  $\hat{I}(Y; L)$  combined with an increase of  $\hat{I}(X; L)$ . Overfitting seems to be more severe in NNs with erf activation functions than in those with ReLU activation functions, and it seems to be more severe in NNs initialized with small weight variances. Similar conclusions regarding overfitting and the impact of the weight variance were obtained for training a two-layer CNN to determine the parity of MNIST digits, albeit on the basis of different qualitative behavior in the IPs, cf. Figs. 2 and 3 in [17].

The authors of [8], [9] considered  $L = \hat{Y}$  to be the output of the NN, i.e.,  $L$  is the index of the largest activation in the final layer. Since  $L$  has finite alphabet,  $I(X; L) = H(L)$  and  $I(Y; L)$  are finite and can be estimated reliably using the plug-in estimator (2). The authors observed that NN training consists of two phases that are entirely different than those in [3]. For all considered architectures, training sets, and activation functions, the authors first observed a strong increase of  $\hat{I}(X; L) = \hat{H}(L)$  followed by a decrease of

$\hat{H}(L|Y)$ , i.e.,  $\hat{I}(Y;L)$  increases more strongly than  $\hat{H}(L)$  in the second phase. Compression does not happen at all: The authors prove that  $\hat{H}(L)$  is bounded from below by an increasing function of training time, cf. Prop. 3 in [9]. In other words, the output of the NN learns about the input throughout training, but starts learning towards the task only if the output contains sufficient information  $\hat{H}(L)$ ; the onset of task-specific learning occurs at larger values of  $\hat{H}(L)$  if label noise is added.

The authors of [6] estimated the (finite) mutual information  $I(X;L)$  in stochastic NNs using the sample propagation estimator from [36]; their estimator was shown to yield qualitatively similar results as a binning estimator of the entropy of  $L$ , i.e., compression in the IP can be explained by geometric compression of the latent representation  $L$ .

Finally, the authors of [16] proposed an estimator based on collisions of a locality sensitive hash function. Specifically, the authors use the plug-in estimators in (2), where the quantizer  $Q$  is a composition of uniform binning and a random non-injective hash function with a uniform density on its range. In their experiments with a  $1024 - 20 - 20 - 20$  MLP trained on MNIST, they observed compression in the hidden layers for both tanh and ReLU activation functions; compression was also observed in a  $200 - 100 - 60 - 30$  MLP and a CNN with ReLU activation functions. For the CNN, the authors did not observe a significant fitting phase, i.e., it appears as if  $\hat{I}(Y;L)$  is large already at the beginning of training or after very few epochs. Since binning plays a major role also for this estimator – points in latent space that are close to each other are mapped to the same hash value – geometric compression is again a possible explanation for the observed reduction of  $\hat{I}(X;L)$ .

#### IV. SUMMARY: COMPRESSION, CLUSTERING, AND GENERALIZATION

We now summarize our analyses from Section III. Although the following statements are not exhaustive, we hope that they help interpreting existing and conducting new research on IP analyses with a better understanding.

- 1) The majority of the literature observes a fitting phase in NN training during which  $\hat{I}(Y;L)$  increases. While NNs with good generalization performance must have large  $I(Y;L)$  as dictated by Fano’s and the data processing inequality, the converse is not true: Large  $I(Y;L)$  does not guarantee that the NN generalizes well; cf. Section 4.3 in [26]. Even less clear is the connection between the estimate  $\hat{I}(Y;L)$  and generalization performance. Indeed, for  $L$  being the softmax output layer and  $\hat{I}(\cdot; \cdot)$  estimated using binning, a three-layer MLP trained on MNIST was shown to have higher  $\hat{I}(Y;L)$  than a six-layer CNN, despite achieving much lower accuracy, cf. Tab. 4 in [10].
- 2) If  $\hat{I}(Y;L)$  is estimated from a test or validation set, then overfitting appears to be visible in the IP as an increase of  $\hat{I}(Y;L)$  followed by a decrease of  $\hat{I}(Y;L)$ .
- 3) A compression phase in NN training during which  $\hat{I}(X;L)$  decreases is not as common as initial claims would suggest, cf. Table I. Furthermore, even if compression occurs in the IP, we believe that the underlying

phenomenon is not information-theoretic. Rather, we believe that compression is geometric in the sense that the NN function  $f$  maps  $\mathcal{D}$  to clusters in latent space, or that the diameter of  $f(\mathcal{D})$  is small. Doubly saturating activation functions encourage clustering because activation values saturate. Weight decay encourages small weights, effectively restricting the diameter of  $f(\mathcal{D})$ . Finally, adding noise to neuron outputs appears to encourage large distances between data points of different classes. That for these stochastic NNs the mutual information  $\hat{I}(X;L)$  indeed measures geometric compression is supported by considering results of training stochastic NNs with  $I(X;L)$  as a regularization term. In such NNs, the latent representations indeed appear clustered, cf. Fig. 2 in [23] and Fig. 1 in [25].

- 4) The convolutional layers of CNNs appear to behave as invertible functions  $f$  at all training epochs:  $\hat{I}(Y;L)$  is large and  $\hat{I}(X;L)$  is close to  $\log |\mathcal{D}|$  throughout entire training. (The analysis in [15] based on MINE is an exception to this.) Invertibility is not in conflict with good generalization performance, cf. [28], [29].
- 5) Consequently, it is neither sufficient nor necessary for good generalization performance that  $L$  is a *minimum* sufficient statistic for  $Y$ , with minimality measured by  $\hat{I}(X;L)$ .
- 6) While compression in the IP can be reasonably explained by geometric compression, geometric compression is not necessary for good generalization performance. For example, the setting visualized in Fig. 5b in [6] achieves top classification performance despite lacking geometric clustering. Whether class-specific clustering is sufficient is unclear, but seems plausible.

Concluding, IP analyses do not entirely live up to their expectations. While fitting and overfitting appear to have counterparts in the IP, a connection between compression in the IP and generalization performance seems highly questionable given the current state of knowledge, cf. Table I. Nevertheless, we believe that the IP has the potential to “open the black box of deep learning” in certain aspects. Taking the properties of the mutual information estimation into account, IP analyses are a valid way to investigate geometric phenomena during NN training, such as geometric compression or class separation. Being able to summarize these geometric properties of an entire layer with just two numbers per epoch, the IP thus yields insights into the effects of regularization and learning schemes that are not available from test set accuracies or learning curves.

#### REFERENCES

- [1] N. Tishby and N. Zaslavsky, “Deep learning and the information bottleneck principle,” in *Proc. IEEE Information Theory Workshop (ITW)*, Jerusalem, Apr. 2015, pp. 1–5.
- [2] M. Vera, P. Piantanida, and L. R. Vega, “The role of the information bottleneck in representation learning,” in *Proc. IEEE Int. Sym. on Information Theory (ISIT)*, Vail, CO, Jun. 2018, pp. 1580–1584.
- [3] R. Shwartz-Ziv and N. Tishby, “Opening the black box of deep neural networks via information,” arXiv:1703.00810 [cs.LG], Mar. 2017.

- [4] A. M. Saxe, Y. Bansal, J. Dapello, M. Advani, A. Kolchinsky, B. D. Tracey, and D. D. Cox, "On the information bottleneck theory of deep learning," in *Proc. Int. Conf. on Learning Representations (ICLR)*, Vancouver, May 2018.
- [5] I. Chelombiev, C. J. Houghton, and C. O'Donnel, "Adaptive estimators show information compression in deep neural networks," in *Proc. Int. Conf. on Learning Representations (ICLR)*, New Orleans, May 2019.
- [6] Z. Goldfeld, E. Van Den Berg, K. Greenewald, I. Melnyk, N. Nguyen, B. Kingsbury, and Y. Polyanskiy, "Estimating information flow in deep neural networks," in *Proc. Int. Conf. on Machine Learning (ICML)*, Long Beach, California, USA, Jun. 2019, pp. 2299–2308.
- [7] M. Schiemer and J. Ye, "Revisiting the information plane," 2019. [Online]. Available: [openreview.net/forum?id=HyljnISFwr](https://openreview.net/forum?id=HyljnISFwr)
- [8] E. R. Balda, A. Behboodi, and R. Mathar, "An information theoretic view on learning of artificial neural networks," in *Proc. Int. Conf. on Signal Processing and Communication Systems (ICSPCS)*, Dec. 2018, pp. 1–8.
- [9] —, "On the trajectory of stochastic gradient descent in the information plane," 2018. [Online]. Available: [openreview.net/forum?id=SkMON20ctX](https://openreview.net/forum?id=SkMON20ctX)
- [10] H. Cheng, D. Lian, S. Gao, and Y. Geng, "Utilizing information bottleneck to evaluate the capability of deep neural networks for image classification," *Entropy*, vol. 21, no. 5, p. 456, May 2019.
- [11] L. N. Darlow and A. Storkey, "What information does a resnet compress?" 2018. [Online]. Available: [openreview.net/forum?id=HklbTjRcKX](https://openreview.net/forum?id=HklbTjRcKX)
- [12] A. Elad, D. Haviv, Y. Blau, and T. Michaeli, "Direct validation of the information bottleneck principle for deep nets," in *Proc. Workshop on Statistical Deep Learning in Computer Vision @ IEEE Int. Conf. on Computer Vision (ICCV)*, Seoul, Oct. 2019.
- [13] H. Fang, V. Wang, and M. Yamaguchi, "Dissecting deep learning networks – visualizing mutual information," *Entropy*, vol. 20, no. 8, p. 823, Aug. 2018.
- [14] M. Gabrié, A. Manoel, C. Luneau, j. barbier, N. Macris, F. Krzakala, and L. Zdeborová, "Entropy and mutual information in models of deep neural networks," in *Proc. Advances in Neural Information Processing Systems (NeurIPS)*, Montreal, Dec. 2018, pp. 1821–1831.
- [15] H. Jónsson, G. Cherubini, and E. Eleftheriou, "Convergence of DNNs with mutual-information-based regularization," in *Proc. Bayesian Deep Learning @ Advances in Neural Information Processing Systems (NeurIPS)*, Vancouver, Dec. 2019.
- [16] M. Noshad, Y. Zeng, and A. O. Hero, "Scalable mutual information estimation using dependence graphs," in *Proc. IEEE Int. Conf. on Acoustics, Speech and Signal Processing (ICASSP)*, May 2019, pp. 2962–2966.
- [17] R. Schwartz-Ziv and A. Alemi, "Information in infinite ensembles of infinitely-wide neural networks," in *Proc. Symp. on Advances in Approximate Bayesian Inference*, Vancouver, Dec. 2019, pp. 1–10.
- [18] K. Wickstrøm, S. Løkse, M. Kampffmeyer, S. Yu, J. Principe, and R. Jenssen, "Information plane analysis of deep neural networks via matrix-based Rényi's entropy and tensor kernels," [arXiv:1909.11396 \[stat.ML\]](https://arxiv.org/abs/1909.11396), Sep. 2019.
- [19] S. Yu, K. Wickstrøm, R. Jenssen, and J. C. Principe, "Understanding convolutional neural networks with information theory: An initial exploration," [arXiv:1804.06537 \[cs.LG\]](https://arxiv.org/abs/1804.06537), Apr. 2018.
- [20] B. Davis, U. Bhatt, K. Bhardwaj, R. Marculescu, and J. Moura, "NIF: A framework for quantifying neural information flow in deep networks," in *Workshop on Network Interpretability for Deep Learning @ AAAI Conf. on Artificial Intelligence (AAAI)*, Honolulu, Jan. 2019.
- [21] D. Choi, K. Lee, C. Shin, and W. Rhee, "On the statistical and information-theoretic characteristics of deep network representations," [arXiv:1811.03666 \[cs.LG\]](https://arxiv.org/abs/1811.03666), Nov. 2018.
- [22] A. Achille and S. Soatto, "Emergence of invariance and disentanglement in deep representations," *Journal of Machine Learning Research*, vol. 19, pp. 1–34, 2018.
- [23] A. A. Alemi, I. Fischer, J. V. Dillon, and K. Murphy, "Deep variational information bottleneck," in *Proc. International Conference on Learning Representations (ICLR)*, Toulon, Apr. 2017.
- [24] A. Achille and S. Soatto, "Information dropout: Learning optimal representations through noisy computation," *IEEE Trans. Pattern Anal. Mach. Intell.*, vol. 40, no. 12, pp. 2897–2905, Dec. 2018.
- [25] A. Kolchinsky, B. D. Tracey, and D. H. Wolpert, "Nonlinear information bottleneck," *Entropy*, vol. 21, no. 11, p. 1181, Nov. 2019.
- [26] R. A. Amjad and B. C. Geiger, "Learning representations for neural network-based classification using the information bottleneck principle," 2019, early access in *IEEE Trans. Pattern Anal. Mach. Intell.*, preprint available: [arXiv:1802.09766 \[cs.LG\]](https://arxiv.org/abs/1802.09766).
- [27] J. Li and D. Liu, "Information bottleneck methods on convolutional neural networks," [arXiv:1911.03722 \[cs.LG\]](https://arxiv.org/abs/1911.03722), Nov. 2019.
- [28] J.-H. Jacobsen, A. W. Smeulders, and E. Oyallon, "i-RevNet: Deep invertible networks," in *Proc. Int. Conf. on Learning Representations (ICLR)*, Vancouver, May 2018.
- [29] B. Chang, L. Meng, E. Haber, L. Ruthotto, D. Begert, and E. Holtham, "Reversible architectures for arbitrarily deep residual neural networks," in *Proc. AAAI Conf. on Artificial Intelligence*, New Orleans, Feb. 2018.
- [30] H. Cheng, D. Lian, S. Gao, and Y. Geng, "Evaluating capability of deep neural networks for image classification via information plane," in *Proc. European Conf. on Computer Vision (ECCV)*, Munich, Sep. 2018, pp. 181–195.
- [31] D. Messerschmitt, "Quantizing for maximum output entropy (corresp.)," *IEEE Transactions on Information Theory*, vol. 17, no. 5, pp. 612–612, Sep. 1971.
- [32] A. Kolchinsky and B. D. Tracey, "Estimating mixture entropy with pairwise distances," *Entropy*, vol. 19, no. 7, p. 361, Jul. 2017.
- [33] B. Poole, S. Ozari, A. van den Oord, A. A. Alemi, and G. Tucker, "On variational bounds of mutual information," in *Proc. Int. Conf. on Machine Learning (ICML)*, Long Beach, California, USA, Jun. 2019, pp. 5171–5180.
- [34] M. I. Belghazi, A. Baratin, S. Rajeshwar, S. Ozair, Y. Bengio, A. Courville, and D. Hjelm, "Mutual information neural estimation," in *Proc. Int. Conf. on Machine Learning (ICML)*, Stockholm, Jul. 2018, pp. 531–540.
- [35] T. Salimans, A. Karpathy, X. Chen, and D. P. Kingma, "PixelCNN++: Improving the PixelCNN with discretized logistic mixture likelihood and other modifications," in *Proc. Int. Conf. on Learning Representations (ICLR)*, Toulon, Apr. 2017.
- [36] Z. Goldfeld, K. Greenewald, J. Weed, and Y. Polyanskiy, "Optimality of the plug-in estimator for differential entropy estimation under gaussian convolutions," in *Proc. IEEE Int. Symp. on Information Theory (ISIT)*, Paris, Jul. 2019, pp. 892–896.